AIAA JOURNAL
Vol. 42, No. 1, January 2004

Passive Fuel–Air Mixing and Emissions Control via Lobed Injectors

M. G. Mitchell,* O. I. Smith,† and A. R. Karagozian‡
University of California, Los Angeles, Los Angeles, California 90095-1597

This experimental study examined the effects of differing levels of passive fuel–air premixing on flame structures and their associated NO_x and CO emissions. Four alternative fuel injector geometries were explored, three of which had lobed shapes. Prior experimental studies of two of these lobed injector flowfields focused on nonreactive mixing characteristics (Smith, L. L., Majamaki, A. J., Lam, I. T., Delabroy, O., Karagozian, A. R., Marble, F. E., and Smith, O. I., "Mixing Enhancement in a Lobed Injector," *Physics of Fluids*, Vol. 9, No. 3, 1997, pp. 667–678) and emissions measurements in the absence of air confinement [Mitchell, M. G., Smith, L. L., Karagozian, A. R., and Smith, O. I., "Burner Emissions Associated with Lobed and Non-Lobed Fuel Injectors," *Twenty-Seventh Symposium (International) on Combustion*, The Combustion Inst., Pittsburgh, PA, 1998, pp. 1825–1831]. The present studies examined the effects of confinement of the crossflow to reduce the local equivalence ratio as well as the effects of altering the geometry and position of the flameholders to further influence passive fuel–air premixing. NO_x and CO emissions as well as flame photographs and planar laser-induced fluorescence imaging of seeded acetone were used to characterize injector performance and fuel and flame evolution. It was found that, with significant air confinement, forcing a more intimate mixing between fuel and air before ignition and flameholding, both NO_x and CO emissions could be simultaneously reduced under the same operating conditions via this passive flow control technique.

Introduction

THE reduction of pollutants from gas turbine engines has been of increasing interest in recent years, both from the perspective of the reduction of oxides of nitrogen (NO_x) and the reduction in carbon monoxide (CO) in the engine exhaust. The strong temperature dependence of the formation of nitric oxide (NO), coupled with the inhibition of the conversion of CO to CO_2 in cool, fuel-lean regions of the flow, increases the difficulty in simultaneously reducing NO_x and CO emissions.[1–4] The capability to mix fuel and air very rapidly relieves both problems to some extent[5]; it reduces the volume of premixed constituents in one case and discourages stoichiometric diffusion flames in the other. The rapid mixing principle is, in fact, the basis of a number of low NO_x burners examined in recent years, for example, the lean premixed, prevaporized combustor[6,7] and the rich-burn/quick-mix/lean-burn combustor.[8] Yet the lean premixed mode of combustion operation is also sensitive to pressure waves and often displays instabilities, with associated flashback or flame blowout.[4] Active fuel–air mixing and combustion control methods, whereby information within the reactive flowfield is sensed and fed back to fuel and other actuation systems, is also of current interest[4,9,10] and has the potential to achieve stabilized combustion under lean premixed conditions.

The goal of the present study is to examine and quantify the effects of passively controlled fuel–air mixing (as created by specific, fixed fuel injector geometries, flameholder configurations, and flow conditions) on flow and flame structures and on the consequent NO_x and CO emissions. The study is part of a larger program that has examined mixing and combustion processes associated with the lobed fuel injector.[11–14] A lobed fuel injector, shown schematically in Fig. 1, is a device in which very rapid initial mixing of reactants can occur through streamwise vorticity generation,[15] producing high strain rates that can delay ignition at fuel–air interfaces.[16] The injector consists of two parallel, corrugated plates, initially flat, with a ramp angle α representing the spatial growth of the corrugation. Fuel is injected from between the plates into coflowing air. Whereas the configurations under examination in this and previous studies had planar orientations, as in Fig. 1, they may in fact be viewed as a section of a cylindrically oriented, daisy- or petal-shaped injector, analogous to the petal nozzles or mixers studied by Narayanan and Damodaran,[17] for example.

Streamwise vorticity is created in a lobed injector by the oppositely oriented secondary flows that develop along the sides of each of the lobes; these flows roll up into counter-rotating vortical structures oriented in the streamwise direction. The mechanism for rollup in the lobed injector is the same as that for the single-interface lobed mixer[18–22] studied extensively for its applications to turbofan engines as a low-pressure-drop mixer. Combustion experiments in a lobed mixer geometry,[23–25] with large volume flow rates of fuel and oxidizer initially separated by a single-lobed splitter plate, demonstrate that the flame spread angle is double that created by a flat splitter plate, indicating enhanced fuel–air mixing processes and an increased rate of flame propagation. In the case of the lobed fuel injector, the streamwise, counter-rotating vortical structures act to strain fuel–air interfaces bounding the thin (distorted) strip of fuel studied computationally in Refs. 26 and 27. Such interfacial strain potentially delays ignition while assisting with reactant molecular mixing with a low-pressure drop and with elimination of the possibility of flashback and a reduction in lean unstable behavior.

Previous mixing studies for the nonreactive lobed injector flowfield indicate increases in molecular mixing and scalar dissipation or strain rates over a planar geometry for a range of flow conditions.[11] These studies employ planar laser-induced fluorescence (PLIF) imaging of acetone seeded in the nonreactive injectant (CO_2) to quantify local unmixedness and average scalar dissipation rates, from which strain rates are estimated.[28] The studies suggest that the lobed injector flowfield has the potential for simultaneous increases in injectant–air mixing and increases in local scalar dissipation and strain rates in the near field of the injector. Transonic flow experiments similarly indicate the potential for increases in mixing and interfacial strain with a lobed injector geometry as compared with nonlobed configurations.[14]

Presented as Paper 99-2400 at the 35th Joint Propulsion Conference, Los Angeles, CA, 20–24 June 1999; received 23 February 2002; revision received 10 June 2003; accepted for publication 10 June 2003.

*Graduate Student Researcher, Department of Mechanical and Aerospace Engineering; currently Combustion Engineer, Capstone Turbine Corporation, Chatsworth, CA 91311.

†Professor, Department of Mechanical and Aerospace Engineering.

‡Professor, Department of Mechanical and Aerospace Engineering. Associate Fellow AIAA.

The performance of the lobed injector in a reactive environment has been explored in preliminary experiments.[12] These experiments, conducted in a subsonic combustion tunnel, compare the behaviors of different lobed and nonlobed injector flowfields, using movable water-cooled flameholders. The experiments specifically monitored the sensitivities of NO_x and CO emissions from propane–air flame structures to the overall tunnel equivalence ratio. These experiments show that at low fuel flow rates, with combustion tunnel equivalence ratio $\phi_{\text{tunnel}} < 0.45$, there result lower NO_x emissions from the lobed injectors as compared with nonlobed injector emissions. However, under specific operating conditions where the tunnel equivalence ratio is higher (but still operating lean, where $0.55 < \phi_{\text{tunnel}} < 1.0$), NO_x emissions from the lobed injectors actually become higher than for the nonlobed injector. It is speculated that this is possibly due to reduced sooting and, hence, reduced radiative heat losses associated with enhanced mixing[29] by the lobed injector geometry. Moreover, CO emissions are observed to become quite high under the conditions producing the lowest NO and NO_x emissions ($\phi_{\text{tunnel}} < 0.45$). Thus, simply a high degree of lean mixing and a locally high strain alone cannot produce simultaneously low NO_x and low CO emissions, as has also been seen in many other studies.[4,30]

The purpose of the present experiments is to explore systematically the quantification of passive fuel–air mixing via lobed injector flowfields and, as a means of improving emissions peformance, the effects of air confinement and flow conditions. Thus, the study explored alternative geometries for lobed fuel injectors, their operating conditions, the degree of confinement of the crossflow, and the flameholding methodologies for the combustion system. The effects of these parameters on fuel–air mixing, emissions, and flow and flame structure evolution suggested the potential for optimization of the lobed injector configuration for combustion purposes.

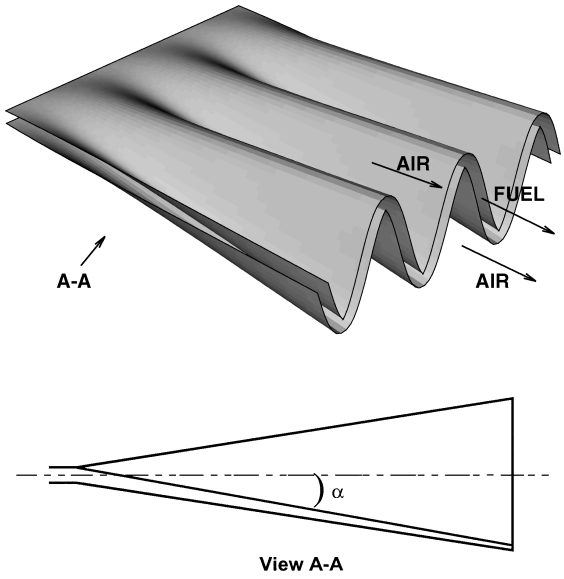

Fig. 1 Schematic of a general lobed injector geometry.

Experimental Facility and Methods

In the present experiments, four different fuel injector geometries were studied in a low-speed, blowdown, atmospheric pressure combustion tunnel. A schematic of the combustion tunnel is shown in Fig. 2. The tunnel's square test section had 9.5-cm sides. A fan was used to drive air through the combustion tunnel at speeds between 2 and 8 m/s in the test section. The tunnel entrance contained a honeycomb section to straighten the flow, followed by a contraction section with a 4:1 area ratio. The tunnel length (measured from the injector exit to the exhaust plenum) was 37.5 cm. Quartz windows were fitted in the two vertical side walls of the test section and at the downstream end of the wind tunnel (in a plane perpendicular to the bulk flow) for optical access. Further details on the combustion tunnel may be found in Refs. 12 and 31.

The four different fuel injectors that were studied in this combustion tunnel had exit plane geometries and dimensions shown in Fig. 3. Lobed injectors A, B1, and C were studied in prior

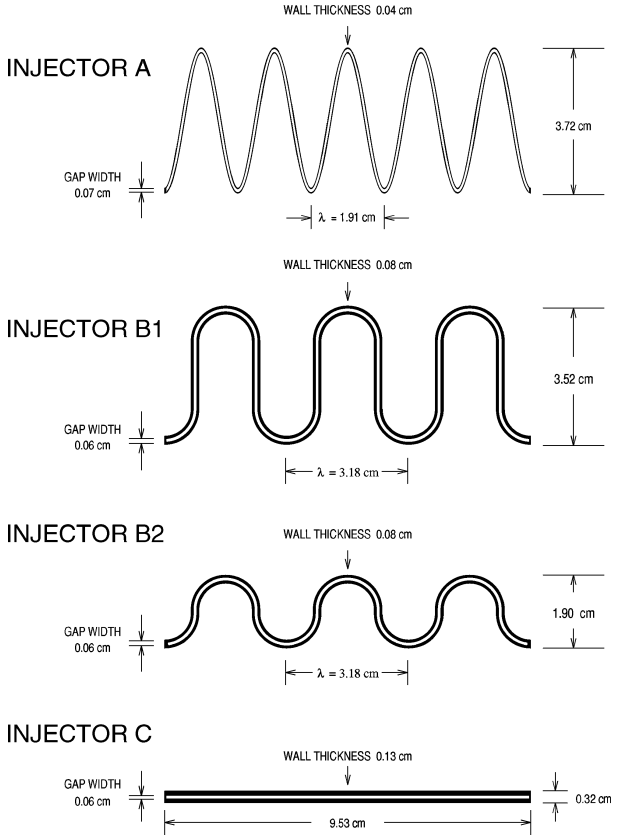

Fig. 3 Exit plane geometries for the four injectors.

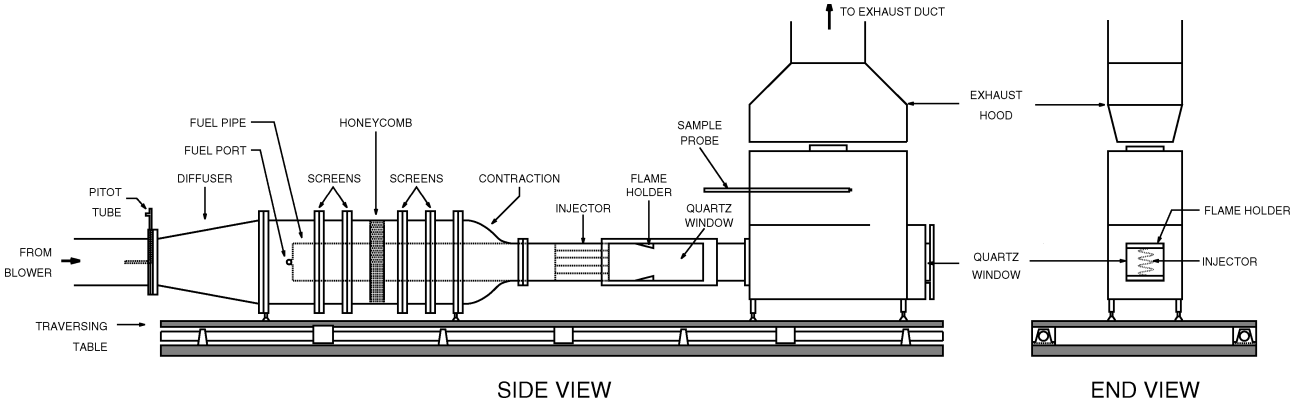

Fig. 2 Schematic diagram of the combustion tunnel and optical access.

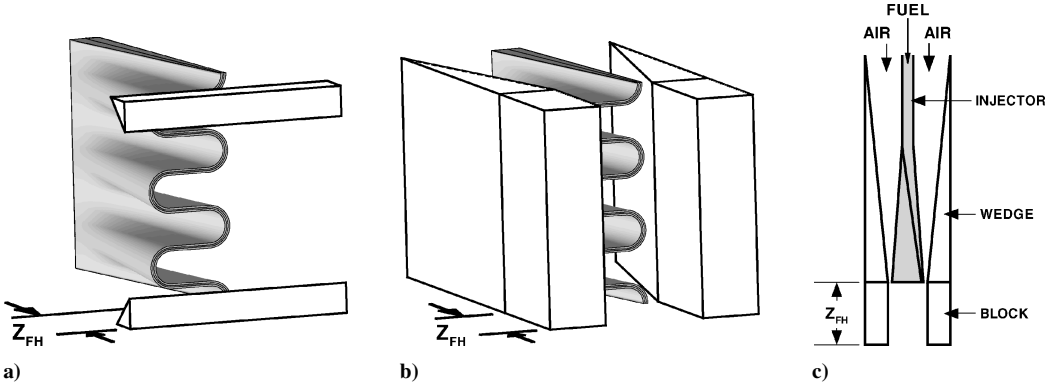

Fig. 4 Alternative injector flowfield and flameholder configurations: a) configuration 1, rearward-facing step flameholders; b) configuration 2, ceramic wedges to confine air coflow in addition to extension blocks, with flameholding at $Z_{FH} \geq 0$; and c) top view schematic of confining wedge and block assembly for configuration 2.

nonreactive[11] and reactive[12] experiments; the latter experiments used the flameholder geometry shown in Fig. 4a. Injector B2 was an alternative fuel injector design, based on the results of numerical simulations of the lobed injector flowfield,[13] which showed a propensity for this shape to generate stronger streamwise vorticity. The lobed injectors were all constructed of aluminum using electric-discharge machining. Injector A was sinusoidal in shape, whereas B1 and B2 consisted of rounded square wave shapes. The injector ramp angle α was approximately 8 deg for injectors A and B1 and 15 deg for injector B2. Fuel injector C was a nonlobed or straight slot injector. As before, we examined this last configuration in an attempt to isolate the effects of the lobes' streamwise vorticity generation on reaction processes and emissions. Propane (C_3H_8) was used in all of the experiments. This fuel is identified by Turns et al.[29] to demonstrate critical levels of air dilution that produce local extrema in NO_x emissions due to the competition among radiative losses, mixing, and residence times.

Several alternative flameholder configurations were used in the present experiments. In some sets of experiments, ramped rearward-facing steps machined from ceramic were placed downstream of the injectors, flush with the upper and lower walls of the test section and oriented perpendicularly with respect to the fuel injector, which was oriented vertically in the tunnel. This configuration is shown in Fig. 4a and is labeled flameholder configuration 1. These rearward-facing step flameholders were fixed at a distance $Z_{FH} = 7$ cm downstream of the exit plane of the fuel injector. These flameholders differed from those used in a prior study,[12] which were water-cooled and made of stainless steel. The present configuration also included ceramic liners at the top and bottom of the tunnel to further reduce heat losses.

In a separate set of experiments, ceramic wedges were placed on either side of the injector as indicated in the two different views shown in Figs. 4b and 4c. Flameholder configuration 2 was examined 1) to confine the coflowing air so that air was less likely to bypass the injected fuel and 2) to increase the likelihood of more complete mixing of fuel and air. These wedges, in addition to ceramic block extensions, were used as effective flameholders. As suggested in Figs. 4b and 4c, flameholder configuration 2 allowed flames to be stabilized nearly at the fuel injector exit in the absence of the block extensions, that is, where $Z_{FH} = 0$, or at a fixed distance from the injector exit via the block extensions, where $Z_{FH} > 0$. In this configuration, the effect of fuel–air premixing before ignition could be examined in detail because of the ability to vary the lengths of the block extensions. The fact that both sets of flameholders were constructed from ceramic enabled the effects of heat losses from the flames to the surroundings to be minimized, or at least to be equivalent between the two present flameholder configurations.

The fuel injectors were each tested in the combustion tunnel for different sets of operating conditions. In the experiments described here, the axial velocities of the airstreams (above and below the injector) were matched, whereas either the fuel exit velocity or the airspeed were varied to produce different overall equivalence ratios for the tunnel. In limited experiments[31] in which the airspeeds above and below the injector were mismatched, allowing the generation of spanwise vorticity as well as streamwise vorticity, there was a quantifiable increase in mixing and a reduction in NO emissions. In all sets of experiments, a chemiluminescent NO–NO_x analyzer (Thermo Electron 10AR Chemiluminescent NO–NO_x Gas Analyzer) was used to measure the NO and NO_2 emissions from the combustor. Calibration of the NO_x analyzer using metered calibration gases suggested relative errors in NO–NO_x measurements of approximately 0.075 or less. Thus, for NO readings in the range of 25 ppm, for example, this error became less than 1 ppm; for the reading range of 10 ppm, the error was less than 0.5 ppm. A nondispersive infrared analyzer was used to measure the CO concentrations (Thermo Environmental Instruments 48C) in the sampled gas stream. Uncertainties in the CO measurements were of the order 1%, so that for most measurements here, the errors were less than 10 ppm. To avoid CO burnout, the single-point probe was water cooled.

Both NO–NO_x and CO measurements utilized single-point probes, fixed at the centerline of the tunnel, near the exhaust section shown in Fig. 2. The locations of the probes were generally downstream of the flame zones, but in rare instances, for example, for a few conditions for lobed injector C, flames did extend beyond the probe. NO_x as well as CO emissions exhibited little spatial variation beyond about 30 cm from the flameholders, and the probes were always placed beyond this point. The region in which CO emissions were measured had relatively low temperatures; temperature measurements in this vicinity suggested rather slow CO reactions. Thus, although residence-time effects were not precisely equal between injector C and the two lobed fuel injector configurations with a fixed probe location, this method was employed because it is commonly used in quantifying emissions in practical engine systems.

Scalar fuel–air mixing was studied in these experiments using PLIF imaging of acetone seeded in the fuel supply as a trace, with virtually the same diffusivity as that of the propane fuel. Acetone was excited with 308-nm laser light from a XeCl excimer laser, pumping several lines in the acetone $A \leftarrow X$ system and resulting in fluorescence proportional to the acetone concentration.[32] The 100-mJ, 25-ns laser beam was formed into a 5-cm-tall sheet, passing through the combustion tunnel test section perpendicular to the direction of bulk flow, with a sheet thickness of 800 μm or less. Nonresonant fluorescence of acetone occurred over a broad spectrum from 350 to 650 nm, peaking at about 435 nm. When the combustion tunnel was moved in the streamwise direction relative to the laser sheet, the evolution of the fuel concentration field driven by the developing vortices was visualized. Only flameholder configuration 1 was used to stabilize flames for this PLIF imaging because of the blockage of light created by the ceramic blocks in configuration 2.

Acetone fluorescence was detected and imaged by an intensified charge-coupled device (CCD) camera located outside the

combustion tunnel's downstream end window. Acetone or fuel evolution was visualized upstream as well as downstream of the flameholders. The images from the CCD camera were acquired and digitized with 512×240 pixels, and the imaging system gave a pixel resolution of better than 130×200 μm. A long-pass glass filter (Schott glass WG 345) was placed in front of the imaging lens to prevent elastically scattered laser light from reaching the intensified CCD array. Background luminosity from the flame was reduced to a negligible proportion of the collected light by gating the image intensifier on for only 500 ns. The short duration of the intensifier gate width also adequately rejected the acetone phosphorescence (200-μs lifetime). Acetone consumption at temperatures above 1000°C occurred only very near the flame zones, as will be seen later. Local mole fractions of acetone/fuel were quantified via PLIF calibration images taken when the combustion tunnel was filled with known acetone concentrations. Pixel values from these images were found to correlate linearly with laser power, acetone concentration, and gain to the camera's intensifier.

An equivalence ratio for the flow in the combustion tunnel overall was defined, as commonly done, by

$$\phi \equiv \frac{(\dot{m}_f/\dot{m}_{\text{air}})}{(\dot{m}_f/\dot{m}_{\text{air}})_{\text{stoich}}} \tag{1}$$

normalizing the mass flow rates of fuel and air, $\dot{m}_f$ and $\dot{m}_{\text{air}}$, with respect to their stoichiometric ratio. Note that this value of ϕ for the combustion tunnel may actually have little direct relevance to the local mass-based fuel–air mixture and associated combustion processes, particularly in light of the alternative flameholders examined. For example, for a given tunnel ratio ϕ_{tunnel}, a local equivalence ratio ϕ_{core} may be estimated by computing ϕ within a rectangular region enclosing only the injector, as shown in Fig. 5a, assuming a uniformly distributed mass flow rate of air over the tunnel cross section. This ϕ_{core} for each injector can be quite different from ϕ_{tunnel}, as suggested by the estimated ϕ_{core} vs ϕ_{tunnel} in Fig. 5b for the different injectors. For example, a stoichiometric tunnel equivalence ratio of $\phi_{\text{tunnel}} = 1.0$ generally corresponded, according to this simple theory, to a very rich-core equivalence ratio $\phi_{\text{core}} = 2.5$, for injectors A and B1, and to ϕ_{core} as high as 5, for injector B2. Injectors A and B1 were relatively similar in amplitude and, hence, had nearly the same relationship between ϕ_{core} and ϕ_{tunnel}. Yet injector B2, because of its smaller amplitude-to-wavelength ratio (with the same fuel flow rate as for the others), created a locally richer flowfield for a given ϕ_{tunnel}. Thus, Fig. 5b implies that all lobed injectors were likely to create a richer local fuel–air mixture, at least near the injection plane, than would be suggested by the tunnel equivalence ratio. However, alternative flameholders, such as flameholder configuration 2, created the possibility for air to be mixed more intimately with fuel without significant air bypassing. This configuration (Figs. 4b and 4c) potentially created much leaner ϕ_{core} values in the center of the tunnel than were created by flameholder configuration 1 (Fig. 4a), for the same value of ϕ_{tunnel}. Hence, the estimated equivalence ratio comparisons shown in Fig. 5b are appropriate to flameholder configuration 1 rather than to configuration 2. The implications of these equivalence ratios will be discussed in the context of emissions results.

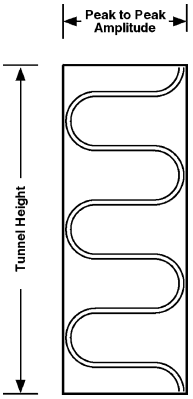

Fig. 5a Schematic diagram of cross-sectional area used for estimation of core equivalence ratio $\phi_{\text{core}} = (\dot{m}_f/\dot{m}_{\text{air}})/(\dot{m}_f/\dot{m}_{\text{air}})_{\text{stoich}}$.

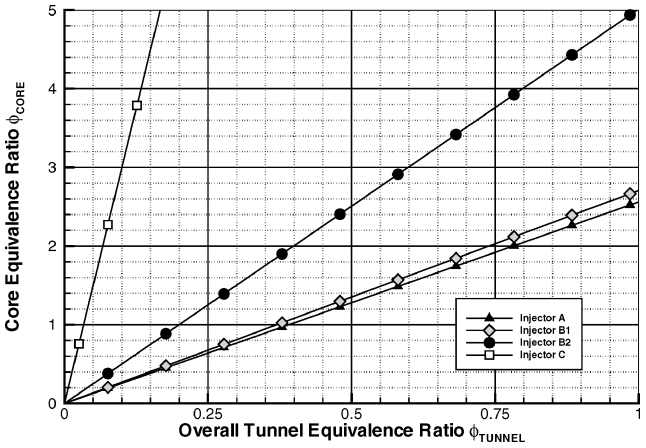

Fig. 5b Estimated ϕ_{core} as a function of the actual tunnel equivalence ratio ϕ_{tunnel}.

Results

The present combustion experiments showed dramatic differences in the visual structure of the flames formed by different injectors in the combustion tunnel. For identical tunnel flow conditions (bulk airspeeds and global equivalence ratios ϕ_{tunnel}), the lobed injector flames stabilized at the flameholders for configuration 1 tended to be highly diffusive and bright blue in color, spanning a large portion of the width of the flameholders. The flames associated with the straight injector C, in contrast, consisted of two distinct diffusion flame sheets, which appeared from the side to be initially laminarlike in structure. Flame structures from both lobed and straight injectors spread toward the walls to become yellow farther downstream, but the sooting levels were always much more pronounced for the straight injector flames. Representative endview photographs of the flames associated with each of the injectors are shown in Fig. 6 for three of the injectors at several different flow conditions. The rearward-step flameholder in these photographs had the geometry of that in Fig. 4a but was water cooled and constructed of stainless steel. The matched bulk airspeeds were 4.5 m/s. Similar behavior was observed for the ceramic flameholders of this geometry. Very lean, blue flames were created by the lobed injectors at the given flow conditions, but highly sooting flames were created by the straight injector. With higher values of ϕ_{tunnel}, the lobed injector flames sooted much more, but never to the extent of sooting by the straight injector. Straight injector flames were in fact substantially longer than those for the lobed injectors; for some operating conditions, they were longer by a factor of two, existing well into the plenum and occasionally into the exhaust section of the combustion tunnel. When flameholder configuration 2 was used with the lobed injectors, on the other hand, for a range of tunnel equivalence ratios the flames appeared to be much shorter, still lean and blue, but much more diffuse than with flameholder configuration 1.

Acetone PLIF images provided a means of visualizing the local fuel distribution through the reaction zone, in planes perpendicular to the mean flow direction, and the fuel's downstream evolution. A minimum of 10 instantaneous PLIF images were averaged to produce each of the temporally averaged spatial distributions of acetone (as a marker for fuel). As an example, Figs. 7a and 7b show the evolution of fuel mole fraction for lobed injector B1, using flameholder configuration 1. Local stoichiometric conditions corresponded to a fuel mole fraction of 0.0418, approximately the transition between blue and green on the color scale shown in Fig. 7. In both sets of data the flameholder (configuration 1) was situated 7 cm downstream of the injector and the matched bulk airspeeds were 4.5 m/s. Figure 7a shows the fuel evolution during cold flow, that is, in the absence of the combustion reaction, for a tunnel equivalence ratio $\phi_{\text{tunnel}} = 0.45$.

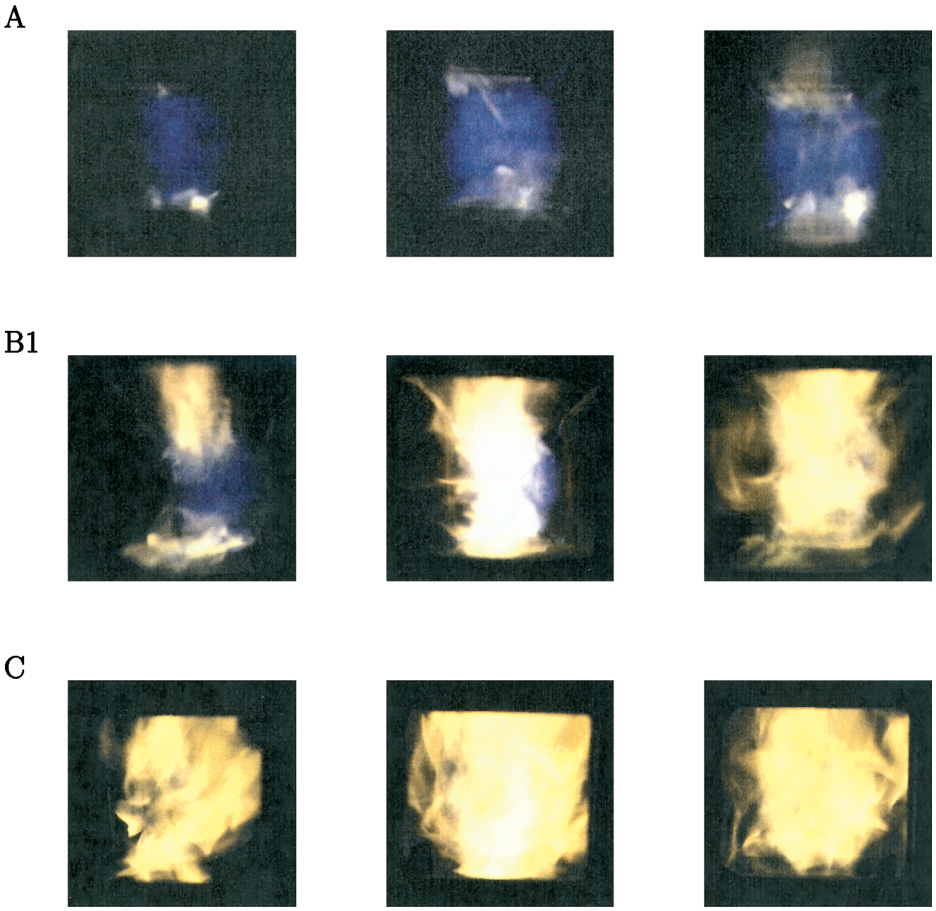

Fig. 6 Photographs of the flames from three different injectors (A1, B1 and C) looking through the end window of the combustion tunnel. In columns from left to right, $\phi_{\text{tunnel}} = 0.35$, $\phi_{\text{tunnel}} = 0.44$, and $\phi_{\text{tunnel}} = 0.53$.

One spurious set of data is noted in Fig. 7a, at a downstream distance of 40 mm. Other than for this single data set, relative errors in the injectant mole fraction were of the order 40–50% for the region $0 < Z < 50$ mm and ranged from 5–20% for the region $Z > 50$ mm. These uncertainties were based on the fluorescence intensity and the injected (measured) propane mixture fraction. Close to the injector, there were so few pixels representing the injected fuel region that uncertainties in fluorescence intensity became much greater than for the region downstream of $Z = 50$ mm. Hence, the PLIF images in Fig. 7 were considered to be more of a qualitative assessment of the fuel-rich regions in the flowfield, rather than a quantitative measure of precise mole fraction.

Figure 7b shows the evolution of fuel imaged during hot reactive conditions, for the same tunnel equivalence ratio. In both Figs. 7a and 7b, the near-field fuel evolution upstream of the flameholder, that is, upstream of $Z_{\text{FH}} = 7$ cm, shows the persistence of the lobed shape and a relatively low level of initial vortex rollup. In fact, the images upstream of 7 cm in Fig. 7a are nearly identical to the corresponding acetone PLIF images in the presence of the combustion reaction, shown in Fig. 7b. This indicates that there was no significant effect of the reaction and associated volumetric heat release on the flowfield upstream of the flameholder. Downstream of 7 cm, the relatively small effects of volumetric expansion on the local lobed injector flow structure evolution were observed in Fig. 7b. As suggested in Fig. 5b, the local mixture created downstream of the injector at $\phi_{\text{tunnel}} = 0.45$ was actually locally rich, even downstream of the flameholders. As verified in Fig. 7b, flame structures only existed at the edges of the rich core of fuel and air, consuming the acetone used to visualize the fuel and burning as a partially premixed, locally rich mode. As a consequence, fuel visualization was possible well downstream of the flameholders during reactive flow. The observed increase in acetone fluorescence intensity for the hot reactive case (Fig. 7b) as compared with the nonreactive case (Fig. 7a) at the same downstream locations was consistent with acetone PLIF studies[33] suggesting increases in fluorescence intensity with temperature. Figure 7b also demonstrates how fuel was drawn from peaks and troughs of the lobed shape toward the inflection zones (middle) of the fuel jet, so that through air entrainment there was a successively leaner mixture created downstream. Yet even at lower tunnel equivalence ratios, for example, $\phi_{\text{tunnel}} = 0.35$, a rich core of fuel and air was observed via acetone PLIF for this lobed injector.[31]

Figures 8 and 9 show results for the emissions (given in parts per million corrected to 15% O_2) of NO, NO_2, NO_x, and CO as a function of the tunnel equivalence ratio ϕ_{tunnel} for different fuel injectors and flameholder configurations. Each data point represents a well-mixed average value of the far-field measurement of concentration, except in a few relatively rich cases for straight injector C, where the probe lay upstream of the diffusion flame end.

Results in Fig. 8 compare emissions from injectors B1, B2, and C, for a fixed flameholder location (configuration 1) 7 cm downstream of the injector and for matched airspeeds of 4.5 m/s. As in prior results with a water-cooled flameholder of a similar geometry,[12] there was a very strong dependence of the lobed injector's NO and overall NO_x emissions on ϕ_{tunnel}, with a lesser dependence on ϕ_{tunnel} for emissions from the straight injector C. The present results, with a ceramic flameholder, yielded slightly higher NO emissions at higher ϕ_{tunnel} for injectors B1 and C than those documented in Ref. 12 with a water-cooled stainless steel flameholder. This observation was consistent with the reduction in heat losses to the surroundings that was accomplished by the ceramic flameholders.

As the lobed injector configuration was changed from B1 to B2, the possible streamwise vorticity generation was increased, and there was somewhat greater fuel–air mixing. However, as noted in Fig. 5b, because of the decreased injector amplitude, the local flowfield for injector B2 became locally richer than for B1, and as a

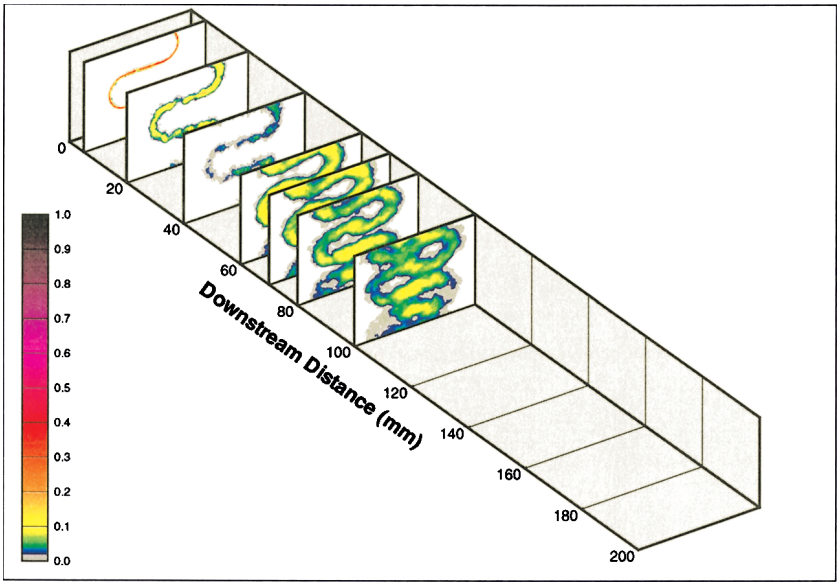

a) Noncombusting flow

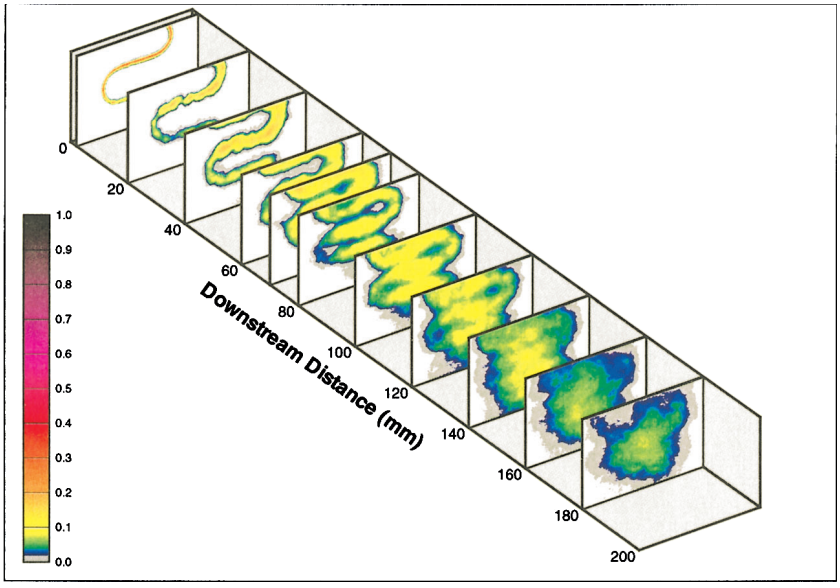

b) Combusting flow

Fig. 7 Downstream evolution of estimated fuel mole fraction field from lobed injector B1 via acetone PLIF at $\phi_{\text{tunnel}} = 0.45$.

consequence, the emissions curves for NO and NO_2 in Fig. 8 shifted slightly to the left for injector B2. This shift indicated that the B2 injector allowed a greater turndown ratio, or capacity for operation at lower ϕ_{tunnel} (0.31 for injector B2, as compared with 0.35 for injector B1). The improved turndown produced the possibility of lower NO emissions for injector B2 than for B1 at very lean conditions. Yet, this also effected a slight increase in NO_2 emissions for injector B2 compared with B1 because the NO_x emissions were nearly the same between the two injectors at low values of ϕ_{tunnel}, although some differences, for example, at $\phi_{\text{tunnel}} = 0.35$, lay beyond the experimental uncertainties. The increase in NO_2 emissions for B2 over those for B1 under locally cool (very lean) conditions was likely the result of the presence of rich pockets of fuel that were distinct from a surrounding blanket of air, as suggested in Fig. 5b. As studied in detail by Hori et al.,[34] small amounts of propane addition during the mixing process between hot combustion gases and cold air can promote the conversion of NO to NO_2. This is consistent with our observation that the richer burning flowfield created by injector B2 produced higher NO_2 emissions than for the slightly leaner flowfield created by B1.

The partial premixing imposed by the lobed injector shape (for either injector B1 or B2) did cause there to be an equivalence ratio dependence in CO emissions, as compared with injector C's CO emissions, which were independent of equivalence ratio. One would expect this type of independence for diffusion flamelike structures as seen for injector C. The improved streamwise vorticity generation and associated mixing produced by injector B2 (as compared with injector B1) did lead to an appreciable reduction in peak CO emissions at low tunnel equivalence ratios, from 1100 ppm for injector B1 at $\phi_{\text{tunnel}} = 0.35$ to 500 ppm for injector B2 at $\phi_{\text{tunnel}} = 0.31$, seen in Fig. 8b. This suggested that improved fuel–air mixing by injector B2, resulting in an additional amount of entrainment of the cool surrounding air into the reaction zone, could act to improve the conversion of CO to CO_2 and, thus, to reduce CO emissions under slightly lowered NO_x conditions. However, the lowest CO emissions at these low equivalence ratios were observed for the straight injector C (of the order 360 ppm at $\phi_{\text{tunnel}} = 0.28$. CO emissions as well as NO_x emissions were in fact generally independent of equivalence ratio for injector C, consistent with the behavior of the diffusion flames that formed for this injector. The lowest CO emissions of all

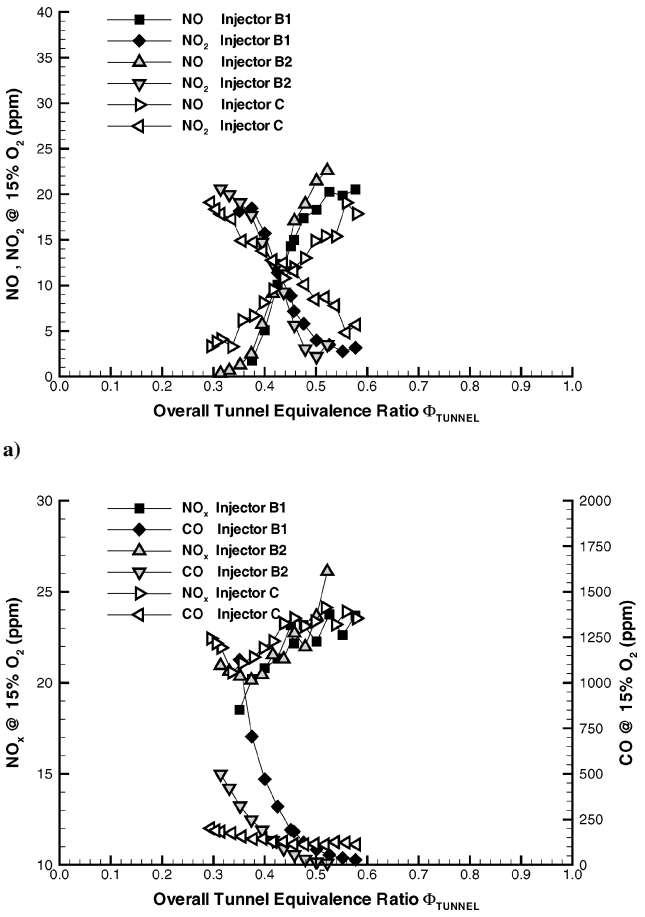

Fig. 8 Emissions of NO, NO_2, NO_x, and CO for lobed fuel injectors B1 and B2 and straight fuel injector C as a function of overall tunnel equivalence ratio ϕ_{tunnel}.

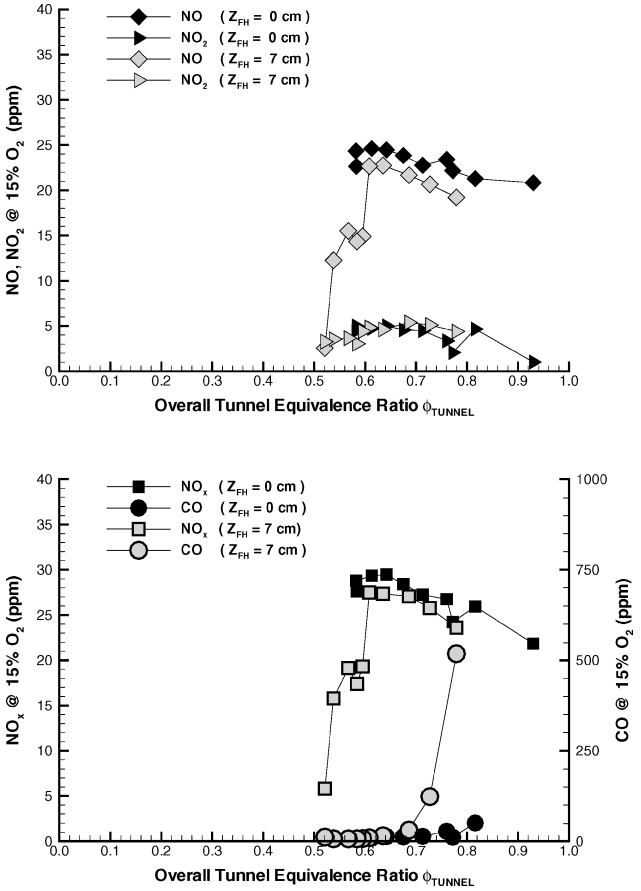

Fig. 9 Emissions of NO, NO_2, NO_x, and CO for lobed fuel injector B1 with different lengths of confinement for the flameholder arrangement in Fig. 4b as a function of normalized tunnel fuel–air mass flux ratio ϕ_{tunnel}.

were achieved by each of the lobed injectors at the higher equivalence ratios (28.2 ppm for injector B1 at $\phi_{\text{tunnel}} = 0.58$ and 10.2 ppm for injector B2 at $\phi_{\text{tunnel}} = 0.52$). Yet these were conditions where the NO_x emissions were not optimized. Clearly, the simultaneous minimization of NO_x and CO emissions was not possible with any of the injector configurations examined for flameholder 1; this flameholder and flowpath arrangement was, thus, deemed to be nonoptimal.

The foregoing observations suggested that altered flow and flameholder configurations shown in Figs. 4b and 4c would have benefits with respect to CO emissions in particular. The altered flowpaths for flameholder configuration 2 were designed to force almost all of the air through the lobed corrugations of the injector, where it could become more fully mixed with the fuel within a relatively short downstream distance. This alternative flowpath was designed as well to reduce or eliminate the rich-fuel pockets clearly evident in the lobed injector flowfield with the original flameholder design (see Figs. 7a and 7b).

The effect of this altered flow and flameholder design on emissions from injector B1, for example, is shown in Fig. 9. Here ϕ_{tunnel} was varied by fixing the fuel flow rate and altering the airflow rate. When only the wedges that end at the injector exit were employed, the flameholder extension blocks were not present; this is designated as the $Z_{\text{FH}} = 0$ flameholder condition. When the extension blocks were employed, the flameholder length Z_{FH} was greater than zero. It was observed that, for the case where $Z_{\text{FH}} = 0$, the NO, NO_2, and NO_x were all relatively constant with respect to varying tunnel equivalence ratio. In this configuration, there was in fact little time for the air and fuel to mix significantly before the flame was ignited and stabilized. Hence, the flame structures visually appeared as diffusion flames emanating from the injector with a lobed shape, yielding relatively constant NO_x emissions, much like the strained diffusion flame produced by injector C. The inadequate mixing of fuel and air before the sudden expansion at $Z_{\text{FH}} = 0$ also decreased the flameholding capabilities of the wedges, and in fact, the diffusion flames began to lift off as the airflow rate was increased and, thus, where ϕ_{tunnel} was reduced. This liftoff prohibited stabilized combustion by the injector for tunnel equivalence ratios below about 0.55. As in the case of straight injector C in Fig. 8, the diffusion flames formed for the $Z_{\text{FH}} = 0$ case in Fig. 9 produced relatively little variation in CO emissions for variable equivalence ratio; this behavior was quite different from that of a premixed flame configuration. The forced air confinement alone appeared to have a benefit with respect to CO emissions for the lobed injector, in that the CO emissions over the range of equivalence ratios was quite low, of the order 7 ppm.

When additional blocks were added to confine the air and move the flameholding farther downstream to $Z_{\text{FH}} = 7$ cm for flameholder configuration 2, visual flame structures suggested much greater and more intimate fuel–air mixing before flameholding. Thus, it was possible to operate at higher airspeeds so that leaner premixed flames could be stabilized in a distributed fashion along the edge of the step formed by the blocks. As a result of burning in a lean premixed mode, Fig. 9 demonstrates that the NO_x emissions were significantly decreased for ϕ_{tunnel} values below about 0.6. For the lowest value of $\phi_{\text{tunnel}} = 0.52$, NO_x emissions dropped to about 6 ppm. Simultaneously, the CO emissions became much lower than CO emissions for the flameholder configuration 1, dropping to the order 12 ppm or less for $\phi_{\text{tunnel}} \leq 0.6$. Confining the air to flow mainly between the lobes virtually eliminated the surrounding blanket of coflowing cold air, thus promoting the oxidation of CO, as shown in Fig. 9. The fact that the CO emissions in this case dropped significantly as ϕ_{tunnel} was reduced was further evidence of the premixed nature of the combustion process with $Z_{\text{FH}} = 7$ cm, as compared with the diffusion flamelike

behavior for $Z_{FH} = 0$ cm. Hence, by confining reactant flow streams to more intimately mix with one another before ignition, we were able to simultaneously produce low NO_x as well as low CO emissions from the lobed injectors. No such simultaneous lowering of emissions was possible from the nonlobed injector C because its emissions performance was limited to that associated with diffusion flames.

Conclusions

These experiments examined the passive control of fuel–air premixing via lobed injector flowfields as well as controlled air confinement and the effects of such mixing control on emissions characteristics. An analysis of mixing and reaction processes was made possible via optical diagnostics. PLIF imaging of a fuel tracer confirmed the distortions of the flowfield by the lobed injector geometry and the tendency toward some fuel–air mixing along lobe sides but with formation of locally fuel-rich, bulk pockets of gas for nonoptimized flameholder configuration 1. This formation of locally mixed regions enabled a reduction in the available turndown ratio for operation of the burner, as compared with that for a nonlobed injector C with diffusion flamelike structures. Although reductions in NO and overall NO_x emissions at relatively lean tunnel equivalence ratios were possible for lobed injector flows, the presence of the surrounding blanket of cool air external to the rich-fuel region resulted in very high CO emissions. Thus, to be able to control and reduce simultaneously, NO_x as well as CO emissions, confinement of the airstream was employed, via an optimized flameholder/flowpath arrangement. This confinement forced a more intimate and complete mixing of fuel and air, creating a much leaner local mixture with stabilized premixed flames, simultaneously emitting very low concentrations of NO, NO_2, and CO. Thus, conditions were identified by which passive premixing and airflow control could lead to very low emissions for both major combustion byproducts through a controlled mixing and flowpath design. Further advantages of this optimal passive control concept include the elimination of lean combustion problems such as flashback and combustion instabilities.

The systematic alteration in fuel injector geometries and flow configurations for emissions reduction had clear benefits in the present study involving the lobed injector. However, broader conclusions may be derived from these studies. Fuel–air mixing enhancement has long been thought[1–3] to lead to ignition delay and the potential for formation of premixed or partially premixed lean flames that can lead directly to lowered NO_x emissions. Yet, the present study suggested that mixing enhancement alone, when there were still cool air regions enveloping the bulk reaction zone, was not sufficient to reduce both NO_x and CO emissions. If one is limited to a passive control scheme such as that with a specific fuel injector geometry, care must be exerted in designing the configuration so that intimate fuel–air mixing as well as the elimination of cool surrounding air regions are promoted. The lobed fuel injector, together with a properly designed flow tailoring and flameholder arrangement, is an example of this type of tightly optimized passive combustion control.

Acknowledgments

The research reported here was supported by NASA Dryden Flight Research Center under Grant NCC-2-374 (S. Corda and K. Iliff, Grant Monitors). The authors acknowledge helpful advice provided by Lance Smith of Precision Combustion, Inc., and by Frank E. Marble of the California Institute of Technology in the initial phases of this study.

References

[1]Bowman, C. T., "Control of Combustion-Generated Nitrogen Oxide Emissions: Technology Driven by Regulation," *Twenty-Fourth Symposium (International) on Combustion*, Combustion Inst., Pittsburgh, PA, 1992, pp. 859–878.

[2]Turns, S. R., "Understanding NO_x Formation in Nonpremixed Flames—Experiments and Modeling," *Progress in Energy and Combustion Science*, Vol. 21, No. 5, 1995, pp. 361–385.

[3]Gore, J. P., and Zhan, N. J., "NO_x Emission and Major Species Concentrations in Partially Premixed Laminar Methane/Air Co-Flow Jet Flames," *Combustion and Flame*, Vol. 105, 1996, pp. 414–427.

[4]Docquier, N., and Candel, S., "Combustion Control and Sensors: A Review," *Progress in Energy and Combustion Science*, Vol. 28, No. 2, 2002, pp. 107–150.

[5]Fric, T. F., "Effects of Fuel–Air Unmixedness on NO_x Emissions" *Journal of Propulsion and Power*, Vol. 9, No. 5, 1993, pp. 708–713.

[6]Fiorentino, A. J., Green, W., Kim, J. C., and Mularz, E. J., "Variable Geometry, Lean, Premixed, Prevaporized Fuel Combustor Conceptual Design Study," *Journal of Engineering for Power*, Vol. 102, 1980, pp. 896–902.

[7]Rokke, N. A., and Wilson, A. J. W., "Experimental and Theoretical Studies of a Novel Venturi Lean Premixed Prevaporized (LPP) Combustor," *Journal of Engineering for Gas Turbines and Power*, Vol. 123, No. 3, 2001, pp. 567–573.

[8]Blomeyer, M., Krautkremer, B., Hennecke, D. K., and Doerr, T., "Mixing Zone Optimization of a Rich-Burn/Quick-Mix/Lean-Burn Combustor," *Journal of Propulsion and Power*, Vol. 15, No. 2, 1999, pp. 288–295.

[9]Pachereit, C. O., Gutmark, E., and Weisenstein, W., "Control of Thermoacoustic Instabilities and Emissions in an Industrial-Type Gas Turbine Combustor," *Proceedings of the Combustion Institute*, Vol. 27, 1998, pp. 1817–1824.

[10]Jackson, M. D., and Agrawal, A. K., "Active Control of Combustion for Optimal Performance," *Journal of Engineering for Gas Turbines and Power*, Vol. 121, 1999, pp. 437–443.

[11]Smith, L. L., Majamaki, A. J., Lam, I. T., Delabroy, O., Karagozian, A. R., Marble, F. E., and Smith, O. I., "Mixing Enhancement in a Lobed Injector," *Physics of Fluids*, Vol. 9, No. 3, 1997, pp. 667–678.

[12]Mitchell, M. G., Smith, L. L., Karagozian, A. R., and Smith, O. I., "Burner Emissions Associated with Lobed and Non-Lobed Fuel Injectors," *Twenty-Seventh Symposium (International) on Combustion*, Combustion Inst., Pittsburgh, PA, 1998, pp. 1825–1831.

[13]Strickland, J. H., Selerland, T., and Karagozian, A. R., "Numerical Simulations of a Lobed Fuel Injector," *Physics of Fluids*, Vol. 10, No. 11, 1998, pp. 2950–2964.

[14]Majamaki, A. J., Smith, O. I., and Karagozian, A. R., "Passive Mixing Control via Lobed Injectors in High-Speed Flow," *AIAA Journal*, Vol. 41, No. 4, 2003, pp. 623–632; also AIAA Paper 2001-3737, July 2001.

[15]Roshko, A., "The Mixing Transition in Free Shear Flows," *The Global Geometry of Turbulence*, edited by J. Jimenez, Plenum, New York, 1991.

[16]Thévenin, D., and Candel, S., "Effect of Variable Strain on the Dynamics of Diffusion Flame Ignition," *Combustion Science and Technology*, Vol. 91, 1993, pp. 73–94.

[17]Narayanan, A. K., and Damodaran, K. A., "Experimental Studies on Piloted Supersonic Combustion Using the Petal Nozzle," *Journal of Propulsion and Power*, Vol. 13, No. 1, 1997, pp. 142–149.

[18]Tillman, T. G., Paterson, R. W., and Presz, W. M., "Flow Structure in a Periodic Axial Vortex Array," AIAA Paper 87-0610, Jan. 1987.

[19]O'Sullivan, M. N., Krasnodebski, J. K., Waitz, I. A., Greitzer, E. M., and Tan, C. S., "Computational Study of Viscous Effects on Lobed Mixer Flow Features and Performance," *Journal of Propulsion and Power*, Vol. 12, No. 3, 1996, pp. 449–456.

[20]Presz, W. M., Morin, B. L., and Gousy, R. G., "Forced Mixer Lobes in Ejector Designs," *Journal of Propulsion and Power*, Vol. 4, No. 4, 1988, pp. 350–355.

[21]Eckerle, W. A., Sheibani, H., and Awad, J., "Experimental Measurements of Vortex Development Downstream of a Lobed Forced Mixer," *Journal of Engineering for Gas Turbines and Power*, Vol. 114, No. 1, 1992, pp. 63–71.

[22]Skebe, S. A., Paterson, R. W., and Barber, T. J., "Experimental Investigation of Three-Dimensional Forced Mixer Lobe Flow Fields," AIAA Paper 88-3785, July 1988.

[23]McVey, J. B., "Observation of the Effect of Streamwise Vorticity on the Spreading of Flames in High Speed Flow," *Combustion Science and Technology*, Vol. 60, 1988, pp. 447–451.

[24]McVey, J. B., and Kennedy, J. B., "Flame Propagation Enhancement Through Streamwise Vorticity Stirring," AIAA Paper 89-0619, Jan. 1989.

[25]Waitz, I. A., and Underwood, D. S., "Effect of Heat Release on Streamwise Vorticity Enhanced Mixing," *Journal of Propulsion and Power*, Vol. 12, No. 4, 1995, pp. 638–645.

[26]Gerk, T. J., and Karagozian, A. R., "Ignition Delay Associated with Strained Fuel Layers," *Twenty-Sixth Symposium (International) on Combustion*, Combustion Inst., Pittsburgh, PA, 1996, pp. 1095–1102.

[27]Selerland, T., and Karagozian, A. R., "Ignition, Burning, and Extinction of a Strained Fuel Strip with Complex Kinetics," *Combustion Science and Technology*, Vol. 131, No. 1–6, 1998, pp. 251–276.

[28]Bish, E. S., and Dahm, W. J. A., "Strained Dissipation and Reaction Layer Analyses of Nonequilibrium Chemistry in Turbulent Reacting Flows," *Combustion and Flame*, Vol. 100, No. 3, 1994, pp. 457–466.

[29]Turns, S. R., Myhr, F. H., Bandaru, R. V., and Maund, E. R., "Oxides of Nitrogen Emissions from Turbulent Jet Flames: Part II—Fuel Dilution and Partial Premixing Effects," *Combustion and Flame*, Vol. 93, 1993, pp. 255–269.

[30]Lefebvre, A. H., *Gas Turbine Combustion*, Hemisphere, New York, 1983, p. 487.

[31]Mitchell, M. G., "Combustion Characteristics of Lobed Fuel Injectors," Ph.D. Dissertation, Dept. of Mechanical and Aerospace Engineering, Univ. of California, Los Angeles, Nov. 2003.

[32]Lozano, A., Yip, B., and Hanson, R. K., "Acetone: A Tracer for Concentration Measurements on Gaseous Flows by Planar Laser-Induced Fluorescence," *Experiments in Fluids*, Vol. 13, 1992, pp. 369–376.

[33]Thurber, M. C., Grisch, F., Kirby, B. J., and Hanson, R. K., "Measurements and Modeling of Acetone Laser-Induced Fluorescence with Implications for Temperature-Imaging Diagnostics," *Applied Optics*, Vol. 37, No. 21, 1998, pp. 4963–4978.

[34]Hori, M., Matsunaga, N., Malte, P. C., and Marinov, N. M., "The Effect of Low-Concentration Fuels on the Conversion of Nitric Oxide to Nitrogen Dioxide," *Twenty-Fourth Symposium (International) on Combustion*, Combustion Inst., Pittsburgh, PA, 1992, pp. 909–916.

J. P. Gore
Associate Editor

Color reproductions courtesy of NASA Dryden Flight Research Center.